Two magnetic orderings and a spin-flop transition in spin-1 system $SrNi_2(PO_4)_2$

Zhangzhen He,[1,3,*] S. C. Chen,[2] C. S. Lue,[2,†] Wendan Cheng,[1] and Yutaka Ueda[3]
[1]*Fujian Institute of Research on the Structure of Matter, Chinese Academy of Sciences, Fuzhou, Fujian 350002, People's Republic of China*
[2]*Department of Physics, National Cheng Kung University, Tainan 70101, Taiwan*
[3]*Institute for Solid State Physics, University of Tokyo, Kashiwa 277-8581, Japan*
(Received 31 May 2008; revised manuscript received 10 November 2008; published 31 December 2008)

Magnetic properties of $SrNi_2(PO_4)_2$ are investigated by means of susceptibility, magnetization, heat-capacity, and ^{31}P NMR measurements. Our experimental results show that $SrNi_2(PO_4)_2$ is a three-dimensional antiferromagnet with two magnetic orderings at ~23 and ~10 K. It is suggested that canted antiferromagnetic ordering at ~23 K may correspond to a Néel noncollinear spin arrangements of Ni^{2+} ions, and such noncollinear spin arrangements further induce spin rotations into a steady collinear antiferromagnetic phase below ~10 K with decreasing temperature. Also, spin-flop transition is observed at a critical field below ~10 K, showing magnetic anisotropy in the system.

DOI: 10.1103/PhysRevB.78.212410 PACS number(s): 75.50.Ee, 75.30.−m

Compounds with a formula of $AM_2(VO_4)_2$ (A=Ba, Sr, Pb; M=Cu, Ni, Co, Mn) have recently attracted much interest due to their unique structural features and rich magnetic properties. Generally, one of their structural features is that all magnetic M^{2+} ions are equivalent with arrays of edge-shared MO_6 octahedra, forming screw chains along the c axis, and the screw chains are separated by nonmagnetic VO_4 (V^{5+}) tetrahedra and A^{2+} ions, resulting in a quasi-one-dimensional (1D) structural arrangement.[1–6] On the other hand, although $AM_2(VO_4)_2$ compounds have similar crystal structures, different magnetic behaviors are clearly found by depending on different magnetic M^{2+} ions from Cu^{2+} to Mn^{2+} ions in the systems. For example, $BaCu_2(VO_4)_2$ exhibits a spin singlet ground state with a large spin gap, which is described as an alternating spin chain or isolated spin dimer system,[7–11] while $SrNi_2(VO_4)_2$ and $PbNi_2(VO_4)_2$ belong to Haldane spin chain systems,[5,12] giving an interesting issue on quantum critical behaviors between spin liquid and Néel ordered states.[13,14] $BaCo_2(VO_4)_2$, $SrCo_2(VO_4)_2$, and $PbCo_2(VO_4)_2$ are Ising spin systems with large magnetic anisotropy,[15–22] showing an interesting field-induced quantum phase transition while $BaMn_2(VO_4)_2$ is found to be canted antiferromagnet with weak ferromagnetism.[23]

In our present study, we try to substitute nonmagnetic P^{5+} for V^{5+} ions of $AM_2(VO_4)_2$ and systematically investigate the changes in the magnetic properties of $AM_2(PO_4)_2$. It is found that $SrCo_2(PO_4)_2$ is a structurally four-spin cluster system, clearly showing the different structural and magnetic properties in contrast to the corresponding vanadate $SrCo_2V_2O_8$.[24] Here, we note that $SrNi_2(PO_4)_2$ is also one of the family $AM_2(PO_4)_2$, which crystallizes in a triclinic structure of space group $P\bar{1}$ with lattice constants of a=5.468(1) Å, b=6.667(1) Å, c=9.156(1) Å, α=110.58(1)°, β=110.87(1)°, and γ=98.01(1)°.[25] As shown in Fig. 1, magnetic Ni ions have two different crystallographic Ni1 and Ni2 sites, and both form dimeric $[Ni_2O_{10}]$ groups via edge sharing. Furthermore, such dimeric $[Ni_2O_{10}]$ groups connect to each other via corner sharing and form a three-dimensional (3D) framework. It is noted that structural features of $SrNi_2(PO_4)_2$ are also different from those of the corresponding vanadate $SrNi_2(VO_4)_2$ with a screw chain structure built by Ni^{2+} ions. In this paper, we first investigate magnetic properties of $SrNi_2(PO_4)_2$ by means of magnetic susceptibility, magnetization, heat-capacity, and NMR measurements. Our results show that $SrNi_2(PO_4)_2$ is a typical three-dimensional antiferromagnet with two magnetic orderings at ~23 and 10 K. Furthermore, a spin-flop transition is also observed at an applied field of ~4 T.

A polycrystalline sample was synthesized by a standard solid-state reaction method using a mixture of high-purity reagents of $SrCO_3$ (4N), $NiC_2O_4 \cdot 2H_2O$ (3N), and $NH_4H_2PO_4$ (3N) as the starting materials in the molar ratio of 1:2:2. The mixture was ground carefully, homogenized thoroughly with ethanol (99%) in an agate mortar, and then packed into an alumina crucible and calcined at 930 °C in air for 40 h with several intermediate grindings. Finally, the product was pressed into pellets and sintered at 950 °C for 20 h, and then cooled to room temperature at a rate of 100 K/h. No impurity phase was observed by powder x-ray diffraction (XRD) measurement using Cu $K\alpha$ radiation. The structural parameters were refined by the Rietveld method using the RIETAN-2000 program,[26] being in good agreement with those reported previously.[25]

Magnetic measurements were preformed using a superconducting quantum interference device (MPMS5S, Quantum Design) magnetometer and heat capacity was measured by a relaxation method using a commercial physical property measurement system (PPMS) (Quantum Design). NMR ex-

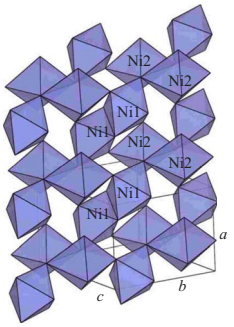

FIG. 1. (Color online) Crystal structure of $SrNi_2(PO_4)_2$ built by Ni^{2+} ions.

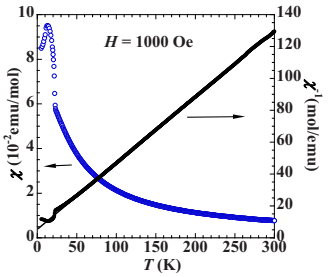

FIG. 2. (Color online) The temperature dependences of the magnetic susceptibility and corresponding reciprocal one of polycrystalline $SrNi_2(PO_4)_2$.

periments were performed using a Varian 300 spectrometer, with a constant field of 7 T. A home-built probe was employed for the low-temperature measurements.[27] The powdered specimen was put in a plastic vial that showed no observable ^{31}P NMR signal. At higher temperatures, the ^{31}P NMR spectra were obtained by the Fourier transform of a half of the spin-echo signal using a standard $\pi/2$-τ-π sequence. On the other hand, the low-temperature spectra were mapped out by integrating the spin-echo signals of various excitations since the resonance lines are extremely broadened.

Figure 2 shows magnetic susceptibility and corresponding reciprocal one of polycrystalline $SrNi_2(PO_4)_2$. The susceptibility increases with decreasing temperature while a rapid increase is observed around ~23 K, suggesting the development of ferromagnetic correlation. A peak is observed around ~15 K, showing the onset of antiferromagnetic (AF) ordering. Above 30 K, susceptibility is followed well by Curie-Weiss behavior, giving the Curie constant $C=2.4(1)$ emu K/mol and Weiss constant $\theta=-13.1(5)$ K. The effective magnetic moment (μ_{eff}) is calculated to be $3.10(4)\mu_B$, which is much larger than the value of $2.82(8)\mu_B$ for $S=1$ with $g=2$. Because Ni^{2+} ions (d^8) do not have a ground-state orbital contribution, such deviations arise likely from mixing with excited orbitally degenerate states of the same spin parity. Also, the negative Weiss constant shows that the dominative interaction exchanges between Ni^{2+} ions are AF.

Figure 3 shows magnetization (M) as a function of applied field (H) at 2 K. A clear change in slope in the magnetization is observed at around 4 T, indicating field-induced magnetic transition. This finding is clearly confirmed by a peak of field derivative of the magnetization (dM/dH). Also,

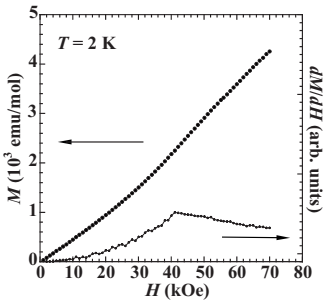

FIG. 3. Magnetization as a function of applied field H at 2 K.

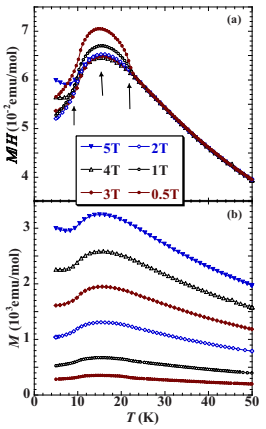

FIG. 4. (Color online) Low-temperature magnetization measured at different fields shown in (a) M/H vs T and (b) M vs T.

no hysteresis and remanent magnetizations are seen in zero field and the magnetization does not saturate up to 7 T.

To identify the nature of magnetic ground state and field-induced magnetic transition of $SrNi_2(PO_4)_2$, the low-temperature susceptibilities and heat capacities are investigated in various magnetic fields. As shown in Fig. 4(a), a rapid increase in susceptibility showing the ferromagnetic correlation appears at ~23 K under a low applied field and then disappears completely when the applied field is larger than 2 T. We suggest that magnetic ordering at ~23 K is likely of canted AF type. For a canted AF system, the total magnetization (M) below T_N can be considered as a sum of the weak ferromagnetic term (M_{WF}) and the linear AF term (χH), $M=M_{\text{WF}}+\chi H$, where M_{WF} arises from canted spins and χH from AF interactions. Therefore, the weak ferromagnetic term M_{WF} is dominative at a lower applied field H, showing a rapid increase in susceptibilities at ~23 K, and the linear AF term becomes gradually dominative with increasing field H, leading to the disappearance of a rapid increase in susceptibilities. Furthermore, no thermal hysteresis in susceptibility around ~23 K between heating and cooling regimes rules out the possibility of structural transition, supporting the onset of canted AF ordering. Moreover, we also note that an upturn in susceptibility below 10 K is observed with increasing applied field. This finding is clearly confirmed in Fig. 4(b), showing a rapid increase in magnetization below 10 K when applied field is larger than 4 T. The result is in good agreement with that observed in M vs H

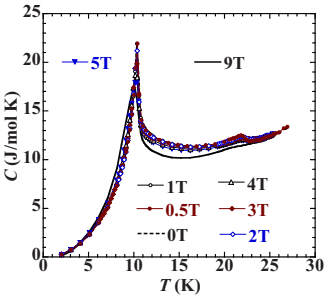

FIG. 5. (Color online) Low-temperature heat-capacity data measured in different fields.

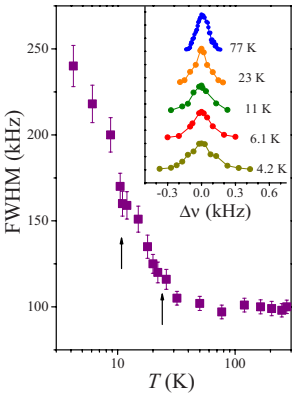

FIG. 6. (Color online) The FWHM of the central line shape as a function of temperature for $SrNi_2(PO_4)_2$. The arrows indicate the antiferromagnetic transition temperatures. The inset shows ^{31}P NMR spectra of $SrNi_2(PO_4)_2$ measured at various temperatures.

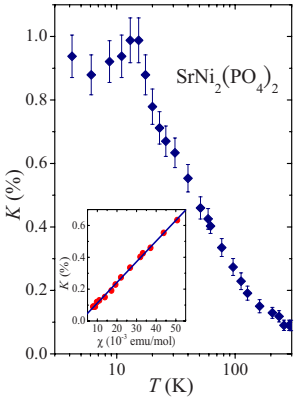

FIG. 7. (Color online) Temperature dependence of the observed ^{31}P NMR shift in $SrNi_2(PO_4)_2$. The inset shows the variation in K versus χ with a solid line indicating the linear relationship.

(Fig. 3), clearly indicating the appearance of field-induced magnetic transition.

Figure 5 shows the heat-capacity data from 50 to 5 K. A jump is seen at around 23 K, agreeing with the temperature of rapid increase in susceptibility. This shows the onset of magnetic ordering at ~23 K. Although rapid increase in susceptibility disappears at the applied field larger than 2 T (Fig. 4), we note that the anomaly at ~23 K in heat capacity does not disappear with increasing field up to 9 T. This finding may support canted AF ordering at ~23 K. Also, a clear λ-like feature is seen at ~10 K, giving concrete evidence for a long-range AF ordering. We note that the temperatures of λ-like peaks do not change with increasing applied field, showing that field-induced magnetic transition is of spin-flop type from AF to AF phases.

To further gain concrete evidence for the existence of two AF orderings in $SrNi_2(PO_4)_2$, we carried out a detailed ^{31}P NMR study invoking the spectrum linewidths, the NMR shifts, as well as the spin-lattice relaxation rates on this compound. The NMR linewidth provides the examination of the magnetic ordering through the magnetic dipolar interaction. The NMR shift is a local measurement of the susceptibility which is less sensitive to the impurities and other phases. The spin-lattice relaxation rate is a sensitive probe for the low-energy spin excitations, revealing dramatic changes in the spin dynamics for the occurrence of magnetic transitions. Regarding the title compound $SrNi_2(PO_4)_2$, a transfer of magnetic $3d$ spin from the nickel ions onto the phosphorus orbital allows us to probe the Ni^{2+} spin dynamics and to determine the magnetic nature through the transferred hyperfine interaction.

As seen in the inset of Fig. 6, the NMR spectra of $SrNi_2(PO_4)_2$ are quite broad at 4.2 K, indicative of the large magnetic dipolar interaction at the phosphorus sites due to the ordered Ni^{2+} moments in the AF state. To have a clear view for the evolution of the line broadening, we display the NMR linewidth as a function of temperature in Fig. 6. It is apparent that the linewidth, measured as the full width at half maximum (FWHM), enhances abruptly below 23 K and continues to increase upon further lowering temperature. This observation is consistent with the bulk results, indicating the first magnetic transition at around 23 K.

Figure 7 shows the result of temperature-dependent NMR shift $K(T)$ for the phosphorus site of $SrNi_2(PO_4)_2$. The value of K was taken at the center of gravity of the resonance line of the measured temperature. The reference frequency here was referred to the ^{31}P resonance frequency of aqueous H_3PO_4. As one can see, the whole temperature variation in K is quite consistent with the susceptibility data, showing a maximum at around 15 K and a small upturn below 6 K. The observed low-T upturn in K provides microscopic evidence for the field-induced magnetic transition in $SrNi_2(PO_4)_2$ with an applied field of 7 T. This is consistent with the results of magnetic data. The NMR shift here is related to the susceptibility by the expression

$$K(T) = \frac{A_{\mathrm{hf}}}{N_{\mathrm{A}}\mu_B}\chi(T),$$

where N_{A} is the Avogadro's constant, μ_B is the Bohr magneton, and A_{hf} is the hyperfine coupling constant due to an intermixing of P and Ni spin states. The observed NMR shift against χ is given in the inset of Fig. 7. The linear behavior indicates a unique hyperfine coupling constant over the en-

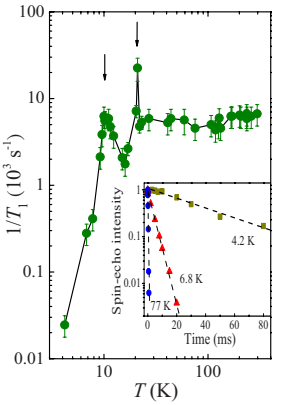

FIG. 8. (Color online) Temperature dependence of the spin-lattice relaxation rate for $SrNi_2(PO_4)_2$. The arrows indicate the antiferromagnetic transition temperatures. The inset shows three representative decay curves taken at 4.2, 6.8, and 77 K, respectively.

tire temperature range that we investigated. The slope yields a value of $A_{hf}=720$ G for $SrNi_2(PO_4)_2$.

To gain more insight into the magnetic characteristics of $SrNi_2(PO_4)_2$, we performed the spin-lattice relaxation rate $(1/T_1)$ measurement, which is sensitive to the low-energy magnetic excitations. It thus provides direct information about the low-energy spin dynamics and the occurrence of magnetic transitions. Here the relaxation-time T_1 measurement was carried out using the saturation recovery method. The saturation of comb with 50 short 2 μs pulses was employed. We recorded the intensity of the ^{31}P spin-echo signal of several delay times. For the nuclear spin $I=1/2$, the decay of the spin-echo signal follows single exponential behavior. Each $1/T_1$ value was thus obtained by fitting to the single exponential function. Three representative spin-echo decay curves taken at 4.2, 6.8, and 77 K are given in the inset of Fig. 8.

The temperature dependence of $1/T_1$ for $SrNi_2(PO_4)_2$ is shown in Fig. 8. It is apparent that $1/T_1$ is almost temperature independent in a wide range at high temperatures. At low temperatures, we found two pronounced peaks in $1/T_1$ at around 23 and 10 K, followed by a rapid decrease below 10 K. The anomalous peaks in $1/T_1$ clearly reflect the change in the spin dynamics, attributed to the presence of magnetic orderings below these two temperatures. The high-temperature constant relaxation rate is a typical feature as the paramagnetic moments fluctuate fast and randomly. Within a localized spin model in a high-temperature limit,[28] the value of $1/T_1$ at a nonmagnetic nucleus can be calculated as

$$\frac{1}{T_1}=\frac{\sqrt{2\pi}(2\gamma_n A_{hf})^2 zS(S+1)}{3\omega_L},$$

where ω_L is the correction frequency of the localized moments given by $\omega_L=k_B|\theta|/\hbar\sqrt{zS(S+1)/6}$ associated with the Weiss constant θ, and the number of the nearest-neighbor coupling between Ni and P ions, z. Taking $\gamma_n=1.083\times10^8$ s^{-1} T^{-1} for the phosphorus nucleus, $A_{hf}=0.072$ T, $\theta=-13.2$ K, $z=6$, and $S=1$ for the spin of Ni^{2+}, the theoretical $1/T_1=2\times10^3$ s^{-1} can be thus estimated. This calculated value is approximately three times smaller than the experimental $1/T_1\sim6\times10^3$ s^{-1}. The discrepancy suggests additional mechanisms such as the orbital fluctuations contributing to the relaxation rate in the paramagnetic state of $SrNi_2(PO_4)_2$. From the NMR results of $SrNi_2(PO_4)_2$, two antiferromagnetic orderings have been confirmed by the presence of marked broadening in the line shape and pronounced peaks in $1/T_1$ near T_N's.

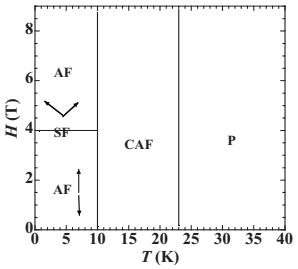

FIG. 9. Phase diagram of $SrNi_2(PO_4)_2$ in the field (H)-temperature (T) plane. AF, CAF, P, and SP represent antiferromagnetic, canted antiferromagnetic, paramagnetic, and spin-flop transition, respectively.

In conclusion, our experimental results of susceptibility, magnetization, heat-capacity, and ^{31}P NMR measurements clearly showed that the system is a 3D antiferromagnet with two magnetic ordering at ~23 and ~10 K. As shown in the phase diagram in the T-H plane (Fig. 9), $SrNi_2(PO_4)_2$ displays a Curie-Weiss behavior at higher temperature and falls into canted AF ordering at ~23 K with lowering temperature. Therefore, weak ferromagnetism may arise from a Néel noncollinear spin arrangements of Ni^{2+} ions. Furthermore, such noncollinear spin arrangements may induce spin rotations into a steady collinear AF phase below ~10 K with decreasing temperature. Below 10 K (T_N), spin-flop transition can be observed at a critical field of ~4 T. In fact, field-induced spin-flop transition may also support a collinear spin arrangement at low temperature and magnetic anisotropy in the system.

One of the authors (Z.H.) acknowledges the Japan Society for the Promotion of Science (JSPS) for financial support. The NMR work was supported by the National Science Council of Taiwan under Grant No. NSC-95-2112-M-006-021-MY3 (C.S.L).

*hcz1988@hotmail.com
†cslue@mail.ncku.edu.tw

[1] R. Wichmann *et al.*, Rev. Chim. Miner. **23**, 1 (1986).
[2] R. Wichmann *et al.*, Z. Anorg. Allg. Chem. **534**, 153 (1986).
[3] R. Vogt *et al.*, Z. Anorg. Allg. Chem. **591**, 167 (1990).
[4] D. Osterloh *et al.*, Z. Naturforsch., B: Chem Sci. **49**, 923 (1994).
[5] Y. Uchiyama *et al.*, Phys. Rev. Lett. **83**, 632 (1999).
[6] M. von Postel *et al.*, Z. Anorg. Allg. Chem. **615**, 97 (1992).
[7] Z. He *et al.*, Phys. Rev. B **69**, 220407(R) (2004).
[8] K. Ghoshray *et al.*, Phys. Rev. B **71**, 214401 (2005).
[9] C. S. Lue *et al.*, Phys. Rev. B **72**, 052409 (2005).
[10] H.-J. Koo *et al.*, Inorg. Chem. **45**, 4440 (2006).
[11] S. S. Salunke *et al.*, Phys. Rev. B **77**, 012410 (2008).
[12] B. Pahari *et al.*, Phys. Rev. B **73**, 012407 (2006).
[13] Z. He *et al.*, J. Phys. Soc. Jpn. **77**, 013703 (2008).
[14] A. Zheludev *et al.*, Phys. Rev. B **62**, 8921 (2000).
[15] Z. He *et al.*, Chem. Mater. **17**, 2924 (2005).
[16] Z. He *et al.*, Phys. Rev. B **72**, 172403 (2005).
[17] Z. He *et al.*, Appl. Phys. Lett. **88**, 132504 (2006).
[18] Z. He *et al.*, Phys. Rev. B **73**, 212406 (2006).
[19] Z. He *et al.*, Solid State Commun. **141**, 667 (2007).
[20] Z. He *et al.*, Solid State Commun. **142**, 404 (2007).
[21] S. Kimura *et al.*, Phys. Rev. Lett. **99**, 087602 (2007).
[22] S. Kimura *et al.*, Phys. Rev. Lett. **100**, 057202 (2008).
[23] Z. He *et al.*, Solid State Commun. **141**, 22 (2007).
[24] Z. He *et al.*, Solid State Commun. **147**, 24 (2008).
[25] B. ElBali *et al.*, J. Solid State Chem. **104**, 453 (1993).
[26] F. Izumi *et al.*, Mater. Sci. Forum **321-324**, 198 (2000).
[27] C. S. Lue *et al.*, Phys. Rev. B **75**, 014426 (2007).
[28] T. Moriya, Prog. Theor. Phys. **16**, 23 (1956).